PAPER • OPEN ACCESS

Bose–Einstein condensates and the thin-shell limit in anisotropic bubble traps

IOP Publishing New J. Phys. 26 (2024) 013035 https://doi.org/10.1088/1367-2630/ad1a29

New Journal of Physics
The open access journal at the forefront of physics

Deutsche Physikalische Gesellschaft DPG
IOP Institute of Physics

Published in partnership with: Deutsche Physikalische Gesellschaft and the Institute of Physics

OPEN ACCESS

RECEIVED
12 September 2023

REVISED
3 December 2023

ACCEPTED FOR PUBLICATION
3 January 2024

PUBLISHED
19 January 2024

PAPER

Bose–Einstein condensates and the thin-shell limit in anisotropic bubble traps

Elias J P Biral[1], **Natália S Móller**[2], **Axel Pelster**[3] **and F Ednilson A dos Santos**[4,*]

[1] Instituto de Física de São Carlos, Universidade de São Paulo, 13560-550 São Carlos, SP, Brazil
[2] RCQI, Institute of Physics, Slovak Academy of Sciences, Dúbravská Cesta 9, 84511 Bratislava, Slovakia
[3] Physics Department and Research Center Optimas, Rheinland-Pfälzische Technische Universität Kaiserslautern-Landau, 67663 Kaiserslautern, Germany
[4] Department of Physics, Federal University of São Carlos, 13565-905 São Carlos, SP, Brazil
[*] Author to whom any correspondence should be addressed.

E-mail: santos@ufscar.br

Keywords: quantum gases, bubble trap, curved manifolds

Abstract

Within the many different models, that appeared with the use of cold atoms to create BECs, the bubble trap shaped potential has been of great interest. However, the relationship between the physical parameters and the resulting manifold geometry remains yet to be fully understood for the anisotropic bubble trap physics in the thin-shell limit. In this paper, we work towards this goal by showing how the parameters of the system must be manipulated in order to allow for a non-collapsing thin-shell limit. In such a limit, a dimensional compactification takes place, thus leading to an effective 2D Hamiltonian which relates to up-to-date bubble trap experiments. At last, the resulting Hamiltonian is perturbatively solved for both the ground-state wave function and the excitation frequencies in the leading order of deviations from a spherical bubble trap.

1. Introduction

In the 1990's, the experimental realization of Bose–Einstein Condensates (BEC) [1, 2] gave rise to a myriad of both theoretical and experimental studies with contributions ranging from a basic understanding of the underlying physics of this macroscopic quantum phenomenon to various applications in particular cases of interest. Among the vast knowledge developed, there is the creation of bubble trap physics [3–7], which consists of thin-shell traps created using a radiofrequency field in an adiabatic potential based on a quadrupolar magnetic trap.

The idea to work with two-dimensional superfluid manifolds soon proved to be appealing to physicists since the fine tune in the geometry opens new possibilities of physical interest. As a natural consequence, many experiments appeared in the literature [8–12]. Unfortunately, there are various technical difficulties in creating bubble trap experiments among which is the gravitational sag, i.e. the sinking of the BEC atoms into the bottom of the trap. With the current developments, it is possible to escape this problem working with microgravity either with free-falling experiments on earth-based laboratories [13, 14] or space-based in the International Space Station (ISS) with the Cold Atom Laboratory (CAL) [15–21]. Up until today, the usual microgravity [22] seems to be the best solution for confining atomic gases into shells in order to study its properties, but some new alternatives such as gravity compensation mechanisms are arising [23, 24]. Also, an interesting substitute to the usual procedure of radio-frequency dressing was proposed for dual-species atomic mixtures [25], which led to the creation of a BEC on Earth's gravity [26].

Confinements in three-dimensional shell shaped condensates inspired some theoretical works worth mentioning here. For instance, in [27], the authors apply analytical methods to investigate the ground state wave function of a BEC and its collective modes. In [28], both analytical and numerical techniques are used in order to obtain expansion properties. The interesting paper [29] employs thermodynamic arguments in order to survey the formation of clusters. The thermodynamics of a BEC on a spherical shell is analyzed, including the critical temperature, in [30–32]. The topological hollowing transition from a full sphere to a

thin-shell was studied in [33, 34], thus finding some universal properties. The ground state and collective excitations of a dipolar BEC was considered in [35]. The general physical relevance of cold atoms on curved manifolds is also addressed in [36]. The contribution of [37] plays with the idea that the external potential is equivalent to the harmonic trap for a large radius thin-shell. Universal scaling relations are found for topological superfluid transitions in bubble traps in [38]. And non-Hermitian phase transitions are meticulously described in [39]. Although it is not the focus of this work, it is also worth citing vortex studies on spherical-like surfaces with no holes [40–47].

In this paper, we work out an explicit relation between the confinement of the particles in the thin-shell limit and the geometrical distortion of a bubble trap for a family of confinement potentials. They are chosen in such a way that the current experiments are included as special cases. All potentials in this family turn out to exhibit the same angular dependency for the confinement strength. Section 2 describes the mathematical background by defining the concepts in which our theory is developed. In a second step we calculate in section 3 the harmonic radial frequency in the Gaussian Normal Coordinate System (GNCS) and expose its resulting angular dependency. Furthermore, the definition of the thin-shell limit is discussed in a more rigorous way by elucidating how it depends on the geometrical distortion of the bubble trap. The general Gross–Pitaevskii Hamiltonian of the system is deduced using a perturbative approach near the thin-shell limit in section 4. In section 5, special topics of the spherical shell and the Thomas–Fermi approximation are considered. Finally, in section 6, the corresponding effective Gross–Pitaevskii equation is perturbatively solved for small distortions from a spherical bubble trap in order to determine both the ground-state wave function and the oscillation frequencies.

2. Gaussian normal coordinate system

In this section, some preliminary concepts are defined and explained in order to establish the mathematical background in which our theory is developed. One of such main concepts concerns the manifold [48, 49] considered here. In this work, we study 2D surfaces embedded into a 3D Euclidean space. More specifically, ellipsoidal surfaces [50–52] are considered since they correspond to the bubble trap potentials in BEC experiments. Therefore, our manifolds are compact, smooth and differentiable everywhere. In order to describe the 3D region around the 2D manifold we choose as a suitable coordinate system, the so-called Gaussian Normal Coordinate System (GNCS) [53, 54]. Further features and particularities on its application can be found in [27].

It is always possible to describe the region around smooth manifolds with the aid of a GNCS. The main idea is to consider two coordinates x^1 and x^2 over the 2D manifold M, also called tangent coordinates, describing arbitrary points in the manifold. Thus, any point $\mathbf{p}$ of this manifold M is portrayed by the position vector $\overrightarrow{p}(x^1,x^2)$. Any point $\mathbf{q}$ in such a vicinity of M can be represented by a coordinate x^0 referred to as the orthogonal coordinate, and a normal unit vector $\hat{n}$ at the point $\mathbf{p}$ through the following equation

$$\overrightarrow{q}\left(x^0,x^1,x^2\right)=\overrightarrow{p}\left(x^1,x^2\right)+x^0\hat{n}\left(x^1,x^2\right). \tag{1}$$

We define the geometrical shape of the manifold in question with the prolate spheroidal coordinates [55, 56]. The transformation equations between such a system of coordinates and the Cartesian System allows us to establish the following family of ellipsoidal surfaces

$$\begin{cases} x=A\sin\nu\cos\phi \\ y=A\sin\nu\sin\phi \\ z=\frac{A}{\sqrt{1+\epsilon}}\cos\nu \end{cases}, \begin{cases} \phi\in[0,2\pi) \\ \nu\in[0,\pi) \end{cases}. \tag{2}$$

Here $\nu=x^1$ and $\phi=x^2$ represent the tangent coordinates, whereas the parameter ϵ stands for the geometrical distortion between an ellipsoid and a sphere according to the equation $x^2+y^2+(1+\epsilon)z^2=A^2$, where A denotes a quantity analogous to a sphere radius characterizing the overall size of the ellipsoid.

For each point on the manifold M it is possible to determine a pair of mutually orthogonal vectors tangent to the manifold by taking partial derivatives of $\overrightarrow{p}(\nu,\phi)$

$$\begin{cases} \vec{v}_1(\nu,\phi)=\frac{\partial\overrightarrow{p}(\nu,\phi)}{\partial\nu}=A\cos\nu\cos\phi\hat{x}+A\cos\nu\sin\phi\hat{y}-\frac{A}{\sqrt{1+\epsilon}}\sin\nu\hat{z}, \\ \vec{v}_2(\nu,\phi)=\frac{\partial\overrightarrow{p}(\nu,\phi)}{\partial\phi}=-A\sin\nu\sin\phi\hat{x}+A\sin\nu\cos\phi\hat{y}. \end{cases} \tag{3}$$

In this way the unitary normal vector can be written as

$$\hat{n}=\frac{\vec{v}_1\times\vec{v}_2}{|\vec{v}_1\times\vec{v}_2|}=\frac{\sin\nu\cos\phi\hat{x}+\sin\nu\sin\phi\hat{y}+\sqrt{1+\epsilon}\cos\nu\hat{z}}{\sqrt{1+\epsilon\cos^2\nu}}. \tag{4}$$

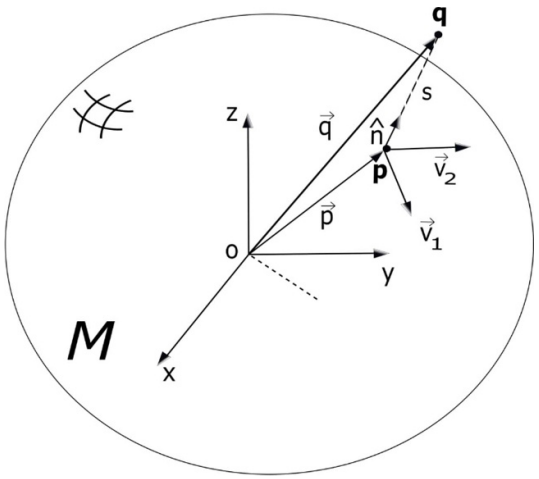

Figure 1. Drawing of the manifold M as an ellipsoid including the GNCS with $(x^0, x^1, x^2) = (s, \nu, \phi)$ described with the aid of the prolate spheroidal coordinates developed in this section.

These vectors form an orthogonal basis according to the following properties

$$\hat{n} \cdot \hat{n} = 1, \quad \vec{v}_1 \cdot \hat{n} = 0, \quad \vec{v}_2 \cdot \hat{n} = 0, \quad \vec{v}_1 \cdot \vec{v}_2 = 0. \tag{5}$$

Choosing $x^0 = s$, the set of coordinates $(x^0, x^1, x^2) = (s, \nu, \phi)$ defines the GNCS.

The visualization of the coordinates and vectors outlined in this section is exposed in figure 1. It shows a drawing of the manifold M as an ellipsoid including the GNCS. The vector $\overrightarrow{p}(\nu, \phi)$ points to the point **p** at the manifold, where $s = 0$. Also the two tangent vectors $\vec{v}_1(\nu, \phi)$ and $\vec{v}_2(\nu, \phi)$, as well as the unit normal vector $\hat{n}(\nu, \phi)$ to the manifold at the point **p** are illustrated.

Now, let us consider the 3D metric tensor $G_{\alpha\beta} = \frac{\partial \overrightarrow{q}(s,\nu,\phi)}{\partial x^\alpha} \cdot \frac{\partial \overrightarrow{q}(s,\nu,\phi)}{\partial x^\beta}$, which has in matrix notation according to the properties (5) the typical form within GNCS

$$G_{\alpha\beta} = \begin{bmatrix} 1 & 0 & 0 \\ 0 & \left(\cos^2\nu + \frac{\sin^2\nu}{1+\epsilon}\right)\left(A + s\frac{1+\epsilon}{(1+\epsilon\cos^2\nu)^{3/2}}\right)^2 & 0 \\ 0 & 0 & \sin^2\nu\left(A + s\frac{1}{\sqrt{1+\epsilon\cos^2\nu}}\right)^2 \end{bmatrix}. \tag{6}$$

It is important to realize that in the case of a spherical shell, with $\epsilon = 0$, we recover the result of the metric tensor for spherical coordinates, where $r = A + s$ denotes the radial coordinate and ν stands for the polar angle.

3. Thin-shell limit for bubble traps

In this section, we discuss the types of potentials that are relevant to this work. Namely, we consider a family of 3D potentials which are constant and have their lowest value along the manifold M, and that have their confinement strength proportional to the geometrical distortion of the ellipsoid. Later we show how such conditions are consistent with actual experimental potentials.

3.1. Confinement potential in a bubble trap

The initial idea is to introduce a parameter Λ, which controls the strength of the confinement in the direction perpendicular to the manifold. To this end, we simplify the notation according to $(x^0, x^1, x^2) \equiv (s, x^i)$ with $i = 1, 2$, so the general potential can be considered as

$$V(s, x^i) \quad = \Lambda^2 v(s, x^i), \tag{7}$$

where the limit $\Lambda \to \infty$ corresponds to an infinitely tight potential thus defining the thin-shell limit. In addition, the factor $v(s, x^i)$ does not depend on the shell thickness and must be chosen in such a way that it fulfills the requisites of being constant at the manifold M and having a vanishing first derivative with respect to s for $s = 0$. Notice that due to the dimension of Λ, $v(s, x^i)$ does not necessarily have dimension of energy. In this section, additional considerations on the definition of the thin-shell limit will be analyzed by relating it to the geometrical distortion of the shell.

In order to study the vicinity of the manifold M, let us start with a Taylor expansion along the orthogonal direction

$$v\left(s,x^i\right) = K + \frac{1}{2!}s^2\left.\frac{\partial^2 v\left(s,x^i\right)}{\partial s^2}\right|_{\mathrm{M}} + O\left(s^3\right), \tag{8}$$

with $K = v|_{\mathrm{M}}$ being a constant at the minimum M, which is characterized by $s = 0$, and the first derivative in s vanishes there. The second derivative of the potential, in the case of the bubble trap, defines the harmonic frequency $\Lambda\Omega$ around the vicinity of the shell. Such derivative follows from

$$\left.\frac{\partial^2 v\left(s,x^i\right)}{\partial s^2}\right|_{\mathrm{M}} = \sum_{\alpha,\beta=1}^{3}\left.\frac{\partial^2 v(x,y,z)}{\partial r^\alpha \partial r^\beta}\right|_{\mathrm{M}} n^\alpha n^\beta = \hat{n}\cdot\left(\nabla\nabla v(x,y,z)\,|_{\mathrm{M}}\right)\cdot\hat{n} = m\Omega^2(x,y,z), \tag{9}$$

where m defines the mass of the particles, $r^1 = x$, $r^2 = y$, $r^3 = z$ represent the Cartesian coordinates, and n^α, n^β denote the respective components of the normal vector. Observe that Ω does not have the same dimension as the harmonic frequency $\Lambda\Omega$, due to the prefactor Λ.

In order to take into account the geometry in the usual bubble trap experiments [4, 5, 8–11, 13–21], let us consider the finite factor of our potential in a generalized form as

$$v(x,y,z) \equiv f\left(x^2 + y^2 + (1+\epsilon)z^2\right). \tag{10}$$

In this case the geometry of the potential is well established to be an ellipsoidal surface, which becomes spherical for $\epsilon = 0$. Thus, our manifold M is characterized by $x^2 + y^2 + (1+\epsilon)z^2 = A^2$, so we conclude $f(x^2 + y^2 + (1+\epsilon)z^2)|_{\mathrm{M}} = f(A^2) = \text{const.}$ and we have $f'(A^2) = 0$.

With such a general form, let us explicitly calculate $m\Omega^2(s,x^i)$. The derivatives can be written in vector form as $\nabla v(x,y,z)|_{\mathrm{M}}\cdot\hat{n} = f'(x^2+y^2+(1+\epsilon)z^2)[2x\hat{x} + 2y\hat{y} + 2(1+\epsilon)z\hat{z}]|_{\mathrm{M}}\cdot\hat{n}$. With $\hat{n}$ expressed in Cartesian coordinates, we obtain $\nabla v(x,y,z)|_{\mathrm{M}}\cdot\hat{n} = 2f'(A^2)\sqrt{x^2+y^2+(1+\epsilon)^2z^2} = 0$. By working out the second derivatives as well, we read off from (9) that $m\Omega^2(x,y,z) = 4f''(A^2)[A^2 + \epsilon(1+\epsilon)z^2]$, which reduces in terms of the GNCS to

$$m\Omega^2\left(x^i\right) \quad = 4f''\left(A^2\right)A^2\left(1+\epsilon\cos^2\nu\right). \tag{11}$$

This gives the final form for the harmonic frequency $\Lambda\Omega$ considering our generalized potential in form of an ellipsoidal surface with the appropriate constraints. Therefore, the confinement strength turns out to be dependent on the geometrical distortion of the ellipsoid through the dependence on the parameter ϵ. Moreover, the dependence on the angle ν establishes that the confinement varies from the poles to the equator of the ellipsoid. Apart from the mentioned conditions, the function f can be quite general, only with the natural assumption that $f''(A^2) > 0$.

Now, some careful considerations must be made for the thin-shell limit. For infinitely tight potentials, we know in advance, that the motion of particles along the normal direction is restricted to the ground state of an harmonic oscillator with frequency $\Lambda\Omega(x^i)$ which is described by a Gaussian wave function with width $\alpha = \sqrt{\hbar/m\Lambda\Omega}$. In previous works, mainly devoted to the spherical case, some authors defined the thin-shell limit as a rather generic situation, where the radius R of the sphere-shaped trap is much larger than the thickness α of the shell. Since these are not the only length scales in this system, different results can be obtained by either considering $R\to\infty$ or $\alpha\to 0$. For example in [47] the authors considered the situation where $R\to\infty$. In the numerical work [31], the authors made some qualitative comparisons between α and R. In some papers [33–35], the ratio R/α is chosen to be as large as possible without more detailed considerations. The objective in this paper is to consider the specific case $\alpha\to 0$, i.e. the case where α is much smaller than any other length scale of the system. This constitutes a more precise definition of a thin-shell limit, which is equivalent to consider $\Lambda\to\infty$.

As already mentioned, in the thin-shell limit we expect the motion in the normal direction to be confined to the ground state of a harmonic oscillator with frequency $\Lambda\Omega$. Since for the ellipsoidal case, Ω is space dependent, every particle in the system will experience a site-dependent energy due to its confinement. Such an energy is provided by the ground-state energy of a harmonic oscillator with frequency $\Lambda\Omega$, i.e.

$$E = \frac{\hbar\Lambda\Omega}{2} = \frac{\hbar\Lambda}{2}\sqrt{\frac{4f''\left(A^2\right)A^2\left(1+\epsilon\cos^2\nu\right)}{m}}. \tag{12}$$

Here we see that for $\epsilon = 0$, this energy diverges for $\Lambda\to\infty$, thus adding a uniform infinite potential which does not have any consequence for the dynamics of the particles moving in the manifold. However for $\epsilon\neq 0$

the situation changes considerably since the particles would be subjected to an infinite space-dependent potential. Let us for example consider the energy difference between the poles and the equator $\Delta E = E(\nu = 0) - E(\nu = \pi/2)$, for which we find $\Delta E \propto \Lambda$ for any non-vanishing ϵ, which means that it diverges in the thin-shell limit. This would then induce a complete localization of particles either at the poles or at the equator, depending on the sign of ϵ. Thus, in order to restrict our limit to physically acceptable situations, we must consider only the case of small geometrical distortions

$$\epsilon = \Lambda^{-1}\bar{\epsilon}, \tag{13}$$

where $\bar{\epsilon}$ is considered to be finite. By taking into account (13), the induced energy difference then becomes

$$\Delta E = \frac{\hbar}{4}\sqrt{\frac{4f''(A^2)A^2}{m}}\bar{\epsilon} + O\left(\Lambda^{-1}\right), \tag{14}$$

which is finite in the thin-shell limit. For arbitrary values of ν, equation (12) becomes

$$E = \frac{\hbar\Lambda}{2}\sqrt{\frac{4f''(A^2)A^2}{m}} + \bar{\epsilon}\frac{\hbar}{4}\sqrt{\frac{4f''(A^2)A^2}{m}}\cos^2\nu + O\left(\Lambda^{-1}\right). \tag{15}$$

Thus, we recognize that the energy per particle generated due to the compactification process separates into one physically irrelevant infinite site-independent part and a finite site-dependent part. It means that, in the thin-shell limit, each particle is effectively subjected to a compactification potential given by

$$V_{\text{comp}} = \bar{\epsilon}\frac{\hbar}{4}\sqrt{\frac{4f''(A^2)A^2}{m}}\cos^2\nu. \tag{16}$$

In experimental terms, the infinitesimal eccentricity $\epsilon = \Lambda^{-1}\bar{\epsilon}$ corresponds to the situation, where the difference between the larger axis and the smaller axis of the ellipsoid is of the same order of the Gaussian width α. This means that, in order to avoid that the particles collapse to either the poles or the equator, the ellipsoidal eccentricity must be kept within such bounds.

In the next subsections, let us consider an experimental realization of the general potential (10) as a generic example where the theory developed in here can be realized.

3.2. Confinement potential in experiments

In this subsection, we apply the calculations to a particular confinement potential. Note that there are some variations of this potential in the literature that differ in the way the potential is defined, for instance, by including gravity effects or considering frequency anisotropy [4, 5].

Let us consider here the more concrete experimental example in [8] as an application of our theory, where

$$V_{\text{E}}(x,y,z) = \sqrt{\left[V_{\text{trap}}(x,y,z) - \hbar\triangle\right]^2 + \left(\hbar\Omega_{\text{RF}}\right)^2}, \tag{17}$$

with $V_{\text{trap}}(x,y,z) = \omega^2 v_{\text{trap}}(x,y,z) = m\omega^2[x^2 + y^2 + (1+\epsilon)z^2]/2$. Here $\hbar\triangle = \hbar\omega_{\text{rf}} - V_0$ denotes the rf detuning with respect to the rf transition at the center of the magnetic trap, and $\Omega_{\text{RF}} = g\mu_{\text{B}}B_1/2\hbar$ stands for the Rabi frequency of the magnetic field $B_1\cos(\omega_{\text{rf}}t)$ with the Landé factor $g = 1/2$ and the Bohr magneton μ_{B}, whereas ϵ represents the geometrical distortion of the ellipsoid. This potential has a local minimum provided that $V_{\text{trap}}(x,y,z) = \hbar\triangle$ for the state $F = 2$, $m_{\text{F}} = 2$.

Let us express the potential according to equation (7), i.e.

$$V_{\text{E}}(x,y,z) = \omega^2\sqrt{\left[v_{\text{trap}}(x,y,z) - \frac{\hbar\triangle}{\omega^2}\right]^2 + \left(\frac{\hbar\Omega_{\text{RF}}}{\omega^2}\right)^2} = \omega^2 v_{\text{E}}(x,y,z), \tag{18}$$

which defines a function f according to (10), where Λ^2 equals to ω^2 in this particular case. The thin-shell limit for such a potential can be obtained by considering $\omega \to \infty$, $\triangle \to \infty$, and $\Omega_{\text{RF}} \to \infty$, while the radii $\hbar\triangle/\omega^2$ and $\hbar\Omega_{\text{RF}}/\omega^2$ are kept finite. Also $\epsilon\omega$ must be kept finite in order to prevent the collapse of the condensate. The expression for the harmonic frequency $\Lambda\Omega$ according to (11) and considering the GNCS with $A = \sqrt{2\hbar\triangle/m\omega^2}$ reads

$$m\Omega_{\text{E}}^2\left(x^i\right) = \tfrac{2m\triangle}{\Omega_{\text{RF}}}\left(1 + \epsilon\cos^2\nu\right). \tag{19}$$

In more experimental terms, the range of parameters corresponding to the thin-shell limit occur for $\alpha \ll A$. Thus, the thin-shell limit corresponds to the inequality

$$\frac{2\Delta}{\omega} \gg \sqrt{\frac{\Omega_{\mathrm{RF}}}{2\Delta}}, \tag{20}$$

which represents a condition involving all three frequencies Δ, ω, Ω_{RF} of the bubble trap potential (19). Conversely, in order to prevent the collapse of the condensate, we must also have $\epsilon A \sim \alpha$. This leads to the eccentricity

$$\epsilon \sim \sqrt{\frac{\omega}{2\Delta}\sqrt{\frac{\Omega_{\mathrm{RF}}}{2\Delta}}}, \tag{21}$$

which is small due to the inequality (20). Within the thin-shell limit for this particular experimental case equation (7) with the aid of (8) becomes

$$V_{\mathrm{E}}\left(s, x^i\right) = \omega^2\left[\frac{\hbar\Omega_{\mathrm{RF}}}{\omega^2} + \frac{1}{2!}s^2\frac{2m\triangle}{\Omega_{\mathrm{RF}}}\left(1+\omega^{-1}\bar{\epsilon}\cos^2\nu\right) + O\left(s^3\right)\right]. \tag{22}$$

And the corresponding compactification potential follows from equation (16)

$$V_{\mathrm{comp}} = \bar{\epsilon}\frac{\hbar}{4}\sqrt{\frac{2\triangle}{\Omega_{\mathrm{RF}}}}\cos^2\nu. \tag{23}$$

Such expressions confirm that the general theory presented here is well suited to deal with the already created experimental bubble-trap potentials.

In order to provide a concrete example, one can consider ^{87}Rb atoms and the frequencies $\omega = 2\pi \times 173\,\mathrm{Hz}$, $\Delta = 2\pi \times 30\,\mathrm{kHz}$, and $\Omega_{\mathrm{RF}} = 2\pi \times 3\,\mathrm{kHz}$ [19], which amounts to $\alpha = 0.4\,\mu\mathrm{m}$ and $A = 15\,\mu\mathrm{m}$. This fulfills, indeed, the thin-shell limit condition $\alpha \ll A$ and prevents the collapse for the quite small eccentricity $\epsilon \sim 0.027$.

4. Effective Hamiltonian in the thin-shell limit

In this section, we will consider the thin-shell limit for interacting particles. Let us begin with the usual 3D Gross–Pitaevskii Hamiltonian

$$H = \int d^3x\left\{\frac{\hbar^2}{2m}|\nabla\Psi|^2 + V(x,y,z)\,|\Psi|^2 + \frac{g_{\mathrm{int}}}{2}|\Psi|^4\right\}, \tag{24}$$

written in Cartesian coordinates, where V stands for the overall potential and g_{int} represents the interaction parameter. The total number of particles is given by

$$N = \int d^3x\,\Psi^*\Psi. \tag{25}$$

Rewriting the Hamiltonian (24) in the GNCS by using the Laplace–Beltrami form of the Laplace operator yields approximately

$$H \approx \int dx^i \int_{s^-(x^i)}^{s^+(x^i)} ds\sqrt{|g|}\left\{-\frac{\hbar^2}{2m}\Psi^*\left[|g|^{-1/2}\frac{\partial}{\partial s}\left(|g|^{1/2}\frac{\partial\Psi}{\partial s}\right) + |g|^{-1/2}\frac{\partial}{\partial x^i}\left(|g|^{1/2}g^{ij}\frac{\partial\Psi}{\partial x^j}\right)\right]\right.$$
$$\left. + V\left(s, x^i\right)\Psi^*\Psi + \frac{g_{\mathrm{int}}}{2}\Psi^{*2}\Psi^2\right\} \tag{26}$$

with the abbreviation $\int dx^i = \int dx^1 \int dx^2$. Here the reduced covariant 2D metric turns out to be

$$g_{ij} = \begin{bmatrix} \left(\cos^2\nu + \frac{\sin^2\nu}{1+\epsilon}\right)\left(A + s\frac{1+\epsilon}{(1+\epsilon\cos^2\nu)^{3/2}}\right)^2 & 0 \\ 0 & \sin^2\nu\left(A + s\frac{1}{\sqrt{1+\epsilon\cos^2\nu}}\right)^2 \end{bmatrix}, \tag{27}$$

which has only the elements corresponding to the tangent coordinates. The limits of the s integral are chosen in such a way that both $(\Lambda\Omega\mathrm{ms}^{-2})/\hbar \gg 1$ and $(\Lambda\Omega\mathrm{ms}^{+2})/\hbar \gg 1$. This assures that the difference between (24) and (26) decays exponentially for $\Lambda \to \infty$ since $\Psi \sim e^{-[\Lambda\Omega(x^i)\mathrm{ms}^2]/2\hbar}$ in the thin-shell limit.

In order to simplify our calculations, we follow [27] and consider the alternative wave function $\widetilde{\Psi}$

$$\Psi\left(s,x^i\right)=\frac{\left|g_0\left(x^i,\epsilon\right)\right|^{1/4}}{\left|g\left(s,x^i,\epsilon\right)\right|^{1/4}}\widetilde{\Psi}\left(s,x^i\right), \tag{28}$$

where $|g_0(x^i,\epsilon)|=|g(0,x^i,\epsilon)|$. Note that the normalization condition (25) for $\tilde{\Psi}$ then reduces to

$$N \approx \int dx^i\sqrt{|g_0|}\int_{s^-(x^i)}^{s^+(x^i)}ds\tilde{\Psi}^*\tilde{\Psi}. \tag{29}$$

This allows us to use the 2D s-independent Jacobian $\sqrt{|g_0|}$ also for the Hamiltonian

$$\begin{aligned}H\approx&\int dx^i\sqrt{|g_0|}\int_{s^-(x^i)}^{s^+(x^i)}ds\left\{-\frac{\hbar^2}{2m}\gamma^{-1/4}\widetilde{\Psi}^*\frac{\partial}{\partial s}\left[\gamma^{1/2}\frac{\partial}{\partial s}\left(\gamma^{-1/4}\widetilde{\Psi}\right)\right]\right.\\&\left.-\frac{\hbar^2}{2m}|g_0|^{-1/2}\gamma^{-1/4}\widetilde{\Psi}^*\frac{\partial}{\partial x^i}\left[|g_0|^{1/2}\gamma^{1/2}g^{ij}\frac{\partial}{\partial x^j}\left(\gamma^{-1/4}\widetilde{\Psi}\right)\right]+V\left(s,x^i,\epsilon\right)\widetilde{\Psi}^*\widetilde{\Psi}+\frac{g_{\rm int}}{2}\gamma^{-1/2}\widetilde{\Psi}^{*2}\widetilde{\Psi}^2\right\},\end{aligned} \tag{30}$$

where we have introduced $\gamma(s,x^i,\epsilon)=|g(s,x^i,\epsilon)|/|g_0(x^i,\epsilon)|$. As already mentioned, in the thin-shell limit we expect $\widetilde{\Psi}\sim e^{-(\Lambda\Omega ms^2)/2\hbar}$, i.e. $\widetilde{\Psi}$ depends implicitly on Λ. In order to make such a dependency explicit, while maintaining the normalization of Ψ as well as to keep the interaction term finite in the limit $\Lambda\to\infty$, we perform the following scale transformations

$$\begin{cases}s=\Lambda^{-1/2}u,\\ \widetilde{\Psi}=\Lambda^{1/4}\psi;\quad \widetilde{\Psi}^*=\Lambda^{1/4}\psi^*,\\ g_{\rm int}=\Lambda^{-1/2}\bar{g}_{\rm int},\end{cases} \tag{31}$$

that gives us some extra control over the Taylor expansions to be performed inside the integrals. These rescaled quantities are the normal direction s, the wave function ψ, and the particle interaction $g_{\rm int}$.

Introducing the abbreviations $\gamma_1=\partial\gamma/\partial s$, $\gamma_2=\partial^2\gamma/\partial s^2$, we obtain together with (7) and (31) for the Hamiltonian (30)

$$\begin{aligned}H\approx&\int dx^i\sqrt{|g_0|}\int_{\Lambda^{1/2}s^-(x^i)}^{\Lambda^{1/2}s^+(x^i)}du\left\{-\Lambda\frac{\hbar^2}{2m}\psi^*\frac{\partial^2\psi}{\partial u^2}-\frac{\hbar^2}{2m}\left(\frac{3}{16}\frac{\gamma_1^2}{\gamma^2}-\frac{1}{4}\frac{\gamma_2}{\gamma}\right)\psi^*\psi\right.\\&-\frac{\hbar^2}{2m}\gamma^{-1/4}\psi^*|g_0|^{-1/2}\frac{\partial}{\partial x^i}\left[(|g_0|^{1/2}\gamma^{1/2}g^{ij}\frac{\partial}{\partial x^j}\left(\gamma^{-1/4}\psi\right)\right]\\&\left.+\Lambda^2\nu(\Lambda^{-1/2}u,x^i,\Lambda^{-1}\epsilon)\psi^*\psi+\frac{\bar{g}_{\rm int}}{2}\gamma^{-1/2}\psi^{*2}\psi^2\right\}.\end{aligned} \tag{32}$$

Now we can expand both ν and γ in a power series with respect to $\Lambda^{-1/2}$ which yields

$$\begin{aligned}\Lambda^2\nu\left(\Lambda^{-1/2}u,x^i,\Lambda^{-1}\bar{\epsilon}\right)=&\ \Lambda^2K+\Lambda\frac{1}{2!}4f''\left(A^2\right)A^2u^2\\&+\Lambda^{1/2}\frac{1}{3!}\left[8f'''\left(A^2\right)A^3+12f''\left(A^2\right)A\right]u^3+\frac{\bar{\epsilon}}{2!}4f''\left(A^2\right)A^2\cos^2\nu\,u^2\\&+\frac{1}{4!}\left[16f^{IV}\left(A^2\right)A^4+48f'''\left(A^2\right)A^2+12f''\left(A^2\right)\right]u^4+O\left(\Lambda^{-1/2}\right).\end{aligned} \tag{33}$$

Note that we have

$$\gamma=1+O\left(\Lambda^{-1/2}\right), \tag{34}$$

and according to appendix we conclude that

$$\left(\frac{3}{16}\frac{\gamma_1^2}{\gamma^2}-\frac{1}{4}\frac{\gamma_2}{\gamma}\right)=O\left(\Lambda^{-1/2}\right). \tag{35}$$

Note that the presence of the harmonic frequency in (11) considering (13) leads to $m\Omega^2=4f''(A^2)A^2+\Lambda^{-1}\bar{\epsilon}4f''(A^2)A^2\cos^2\nu=m\Omega_0^2+\Lambda^{-1}\bar{\epsilon}m\Omega_0^2\cos^2\nu$, where

$$m\Omega_0^2=4f''\left(A^2\right)A^2. \tag{36}$$

Substituting these equations and neglecting exponentially decaying contributions, the Hamiltonian can be written as $H = H_2 + H_1 + H_{1/2} + H_0 + \mathrm{O}(\Lambda^{-1/2})$, where the respective terms are sorted according to decreasing contributions with

$$H_2 = \Lambda^2 K \int dx^i \int du \sqrt{|g_0|}\psi^*\psi = \Lambda^2 K N, \tag{37}$$

$$H_1 = \Lambda \int dx^i \int du \sqrt{|g_0|}\left(-\frac{\hbar^2}{2m}\psi^*\frac{\partial^2\psi}{\partial u^2} + \frac{1}{2}m\Omega_0^2 u^2\psi^*\psi\right), \tag{38}$$

$$H_{1/2} = \Lambda^{1/2} \int dx^i \int du \sqrt{|g_0|}\left[\frac{4}{3}f'''\left(A^2\right)A^3 + 2f''\left(A^2\right)A\right]u^3\psi^*\psi, \tag{39}$$

$$\begin{aligned} H_0 = \int dx^i \int du \sqrt{|g_0|}\Bigg\{ & -\frac{\hbar^2}{2m}\psi^*|g_0|^{-1/2}\frac{\partial}{\partial x^i}\left(|g_0|^{1/2}g_0^{ij}\frac{\partial}{\partial x^j}\psi\right) + \frac{\bar{\epsilon}}{2}m\Omega_0^2u^2\cos^2\nu\,\psi^*\psi \\ & + \left[\frac{2}{3}f^{IV}\left(A^2\right)A^4 + 2f'''\left(A^2\right)A^2 + \frac{1}{2}f''\left(A^2\right)\right]u^4\psi^*\psi + \frac{\bar{g}_{\mathrm{int}}}{2}\psi^{*2}\psi^2\Bigg\}, \end{aligned} \tag{40}$$

with limits for the integrals in u being $-\infty$ to ∞. Since H_2 turns out to be a simple additive constant, our analysis effectively starts with H_1.

Note that H_1 lacks an interaction term and essentially corresponds to the harmonic oscillator Hamiltonian whose spectrum is given by the linear eigenvalue equation

$$-\frac{\hbar^2}{2m}\frac{\partial^2\psi}{\partial u^2} + \frac{1}{2}m\Omega_0^2u^2\psi = \frac{E_1}{\Lambda}\psi. \tag{41}$$

Therefore, at order Λ^0 the degenerate eigenfunctions of (41) are given by

$$\begin{aligned} \psi_{n,l}^{(0)}\left(u,x^i\right) &= \psi_{n\perp}(u)\,\xi_l\left(x^i\right) \\ &= \frac{1}{\sqrt{2^n n!}}\left(\frac{m\Omega_0}{\pi\hbar}\right)^{1/4}\exp\left(-\frac{m\Omega_0}{2\hbar}u^2\right)H_n\left(\sqrt{\frac{m\Omega_0}{\hbar}}u\right)\xi_l\left(x^i\right), \end{aligned} \tag{42}$$

where H_n denote the Hermite polynomials, $\psi_{n\perp}$ represent the harmonic oscillator eigenstates, and ξ_l stand for arbitrary functions of x^i obeying the condition $\sum_l \int dx^1 \int x^2 \sqrt{|g_0|}\xi_l^*(x^i)\xi_l(x^i) = N$. The dominant contribution to the energy spectrum of the system reads

$$E_n^{(1)} = N\Lambda\hbar\Omega_0\left(\frac{1}{2} + n\right). \tag{43}$$

Therefore, in the thin-shell limit, where we have $\Lambda \to \infty$, the system acquires infinitely separated energy bands. This implies that, physically, only the lowest energy band with energy $E_1 = E_0^{(1)} = N\Lambda\hbar\Omega_0/2$ will be populated with particles, i.e. $\xi_l = 0$ for $l \neq 0$. In particular, the normalization condition for ξ_0 becomes

$$\int dx^i \sqrt{|g_0|}\xi_0^*\left(x^i\right)\xi_0\left(x^i\right) = N. \tag{44}$$

Now, let us deal with the effects of the $H_{1/2}$ contribution to the total Hamiltonian. Similar to H_1, also $H_{1/2}$ acts only in the subspace defined by the variable u. This means that it will induce corrections of order $\Lambda^{-1/2}$ to $\psi_{n\perp}$ as well as corrections of order $\Lambda^{1/2}$ to the energies (43). Such corrections of order $\Lambda^{-1/2}$ to $\psi_{n\perp}$ can be neglected in the thin-shell limit, while the contribution with power $\Lambda^{1/2}$ to (43) vanishes since it involves the infinite integral of an odd function of u according to

$$E_n^{(1/2)} = \Lambda^{1/2}\int dx^i \int_{-\infty}^{+\infty} du\sqrt{|g_0|}\left[\frac{4}{3}f'''\left(A^2\right)A^3 + 2f''\left(A^2\right)A\right]u^3\psi_{n,0}^{*(0)}\psi_{n,0}^{(0)} = 0. \tag{45}$$

Although the contribution to the energy with power $\Lambda^{1/2}$ vanishes, an application of second-order perturbation theory considering $H_{1/2}$ as a perturbation over H_1 shows that contributions with power Λ^0 to (43) do not vanish. In particular the correction $E_0^{(0)}$ to $E_0^{(1)}$ due to $H_{1/2}$ is

$$E_0^{(0)} = -\frac{11N\hbar^2}{18m}\left(\frac{2f'''\left(A^2\right)A^3 + 3f''\left(A^2\right)A}{4f''\left(A^2\right)A^2}\right)^2. \tag{46}$$

Further contributions to (43) due to $H_{1/2}$ are of order $\Lambda^{-1/2}$ and are negligible in the thin-shell limit.

Finally, we must consider the effect of H_0 for the energy spectrum and eigenstates. The first thing to observe is that H_0 also acts over the subspace defined by the coordinates x^i, which implies that H_0 is able to break the degeneracy. Therefore, at order Λ^0 the system is effectively separated into disjoint subspaces, each one having wave functions given by $\psi_{n\perp}(u)\xi_n(x^i)$. According to (43), the energy gap between such subspaces is of the order of Λ, which means that in the thin-shell limit $\Lambda \to \infty$ only the subspace with lowest energy becomes occupied. Consequently, the system wave function in the thin-shell limit must be

$$\psi\left(u, x^i\right) = \left(\frac{m\Omega_0}{\pi\hbar}\right)^{1/4} \exp\left(-\frac{m\Omega_0}{2\hbar}u^2\right) \xi\left(x^i\right), \tag{47}$$

where $\xi(x^i) = \xi_0(x^i)$. Substituting (47) into H_0 and integrating where possible yields the constant contribution

$$C_0 = \frac{N}{8}\frac{\hbar^2}{m}\frac{4f^{IV}\left(A^2\right)A^4 + 12f'''\left(A^2\right)A^2 + 3f''\left(A^2\right)}{4f''\left(A^2\right)A^2} \tag{48}$$

in addition to the effective Hamiltonian

$$H_{\text{eff}} = \int dx^i \sqrt{|g_0|}\left\{-\frac{\hbar^2}{2m}\xi^*|g_0|^{-1/2}\frac{\partial}{\partial x^i}\left(|g_0|^{1/2}g_0^{ij}\frac{\partial}{\partial x^j}\xi\right) + \frac{\bar{\epsilon}}{4}\hbar\Omega_0\cos^2\nu\,\xi^*\xi + \frac{\bar{g}_{2D}}{2}\xi^{*2}\xi^2\right\}. \tag{49}$$

The latter simplifies to

$$H_{\text{eff}} = \int_0^{\pi} d\nu \int_0^{2\pi} d\phi A^2 \sin\nu \left\{-\frac{\hbar^2}{2mA^2\sin\nu}\xi^*\left[\frac{\partial}{\partial\nu}\left(\sin\nu\frac{\partial\xi}{\partial\nu}\right) + \frac{\partial}{\partial\phi}\left(\frac{1}{\sin\nu}\frac{\partial\xi}{\partial\phi}\right)\right] + \frac{\bar{\epsilon}}{4}\hbar\Omega_0\cos^2\nu\,\xi^*\xi + \frac{\bar{g}_{2D}}{2}\xi^{*2}\xi^2\right\}, \tag{50}$$

where the resulting effective interaction strength in 2D turns out to be

$$\bar{g}_{2D} = \left(\frac{m\Omega_0}{2\pi\hbar}\right)^{1/2}\bar{g}_{\text{int}} = \left(\frac{m\Omega_0\Lambda}{2\pi\hbar}\right)^{1/2} g_{\text{int}}. \tag{51}$$

With this, we conclude that (50) is the appropriate Hamiltonian in the thin-shell limit apart from the diverging additive constant $E_2 + E_0^{(1)} + E_0^{(0)} + C_0$.

5. Particular cases

Evaluating the functional derivative of the effective Hamiltonian (50), it is possible to obtain the wave function that minimizes it. To this end, however, we have to take into account the constraint (44) and its corresponding Lagrange multiplier, the chemical potential μ according to

$$\frac{\delta H_{\text{eff}}}{\delta\xi^*\left(x^i\right)} - \mu\frac{\delta N}{\delta\xi^*\left(x^i\right)} = 0, \tag{52}$$

which finally leads to

$$-\frac{\hbar^2}{2mA^2\sin\nu}\left[\frac{\partial}{\partial\nu}\left(\sin\nu\frac{\partial\xi}{\partial\nu}\right) + \frac{\partial}{\partial\phi}\left(\frac{1}{\sin\nu}\frac{\partial\xi}{\partial\phi}\right)\right] + \frac{\bar{\epsilon}}{4}\hbar\Omega_0\cos^2\nu\xi + \bar{g}_{2D}\xi^*\xi^2 = \mu\xi. \tag{53}$$

Let us consider now some particular cases for this 2D time-independent GPE.

5.1. Spherical shell

At first we deal with the particular situation of the spherical shell, i.e. $\bar{\epsilon} = 0$, which allows some simplifications. Most importantly, the wave function corresponding to the lowest energy state $\xi(x^i)$ is a constant along the shell, since the BEC particles are uniformly distributed around the bubble. Let us determine the constant value of ξ through the normalization (44), which yields for the ground state of the system

$$\xi = \sqrt{\frac{N}{A^2 4\pi}}. \tag{54}$$

Substituting this value for the wave function into the effective Hamiltonian (50), we find with $\bar{\epsilon} = 0$ the corresponding energy

$$E_S = \frac{\bar{g}_{2D}}{8A^2\pi} N^2. \tag{55}$$

This is the Λ^0 contribution to the energy for the spherical shell. Thus, the total ground-state energy amounts in this case to $E_2 + E_0^{(1)} + E_0^{(0)} + C_0 + E_S$, which is consistent with reference [28].

5.2. Thomas–Fermi approximation

For situations, where the interaction energy is much larger than the kinetic energy, the so-called Thomas–Fermi approximation can be applied. In case of the effective Hamiltonian 50, this corresponds to the situation where $N \to \infty$ or $A \to \infty$. In order to calculate the wave function $\xi(x^i)$, we take (53) without the kinetic energy term, which gives

$$\xi = \sqrt{\frac{\mu - \frac{\bar{\epsilon}}{4}\hbar\Omega_0 \cos^2\nu}{\bar{g}_{2D}}}. \tag{56}$$

As expected, $\xi(x^i)$ has an angular dependence along the shell. Inserting it into equation (50) and solving the integral, we find the Thomas–Fermi energy

$$E_{TF} = \frac{\pi A^2 \left(80\mu^2 - \bar{\epsilon}^2\hbar^2\Omega_0^2\right)}{40\bar{g}_{2D}}, \tag{57}$$

which represents the ground state Λ^0 energy contribution without the diverging additive constants. Taking into account (44), it can be rewritten in terms of the total number of particles N as

$$E_{TF} = \frac{\pi A^2}{40\bar{g}_{2D}} \left(\frac{5\bar{g}_{2D}^2 N^2}{\pi^2 A^4} + \frac{10}{3\pi A^2} \bar{g}_{2D} N \bar{\epsilon}\hbar\Omega_0 - \frac{4\bar{\epsilon}^2\hbar^2\Omega_0^2}{9} \right). \tag{58}$$

Thus, the total ground-state energy in this case is $E_2 + E_0^{(1)} + E_0^{(0)} + C_0 + E_{TF}$, which is also consistent with reference [28].

6. Perturbative solutions

Although the main result of our work is the step-by-step construction of the theory for BECs in the thin-shell limit of a bubble trap, this paper also provides solutions to particular cases of the spherical shell and the Thomas–Fermi regime for the effective Hamiltonian (50), thus revealing some mathematical aspects of the corresponding wave functions. Now, in this chapter, we determine both the ground-state wave function and the excitation frequencies perturbatively by considering the geometrical distortion $\bar{\epsilon}$ as the smallness parameter.

6.1. Perturbative ground state

Let us now perturbatively solve (53), which we rewrite as

$$\frac{1}{2mA^2}\hat{L}^2\xi + \lambda\cos^2(\nu)\,\xi + \bar{g}_{2D}\,|\xi|^2\,\xi = \mu\,\xi, \tag{59}$$

where we have introduced the smallness parameter $\lambda = \bar{\epsilon}\hbar\Omega_0/4$. In the following, we also have to take into account the normalization (44), which reads explicitly $\int dS\,|\xi|^2 = A^2\int_0^{2\pi} d\phi \int_0^{\pi} d\nu\, \sin\nu\, |\xi|^2 = N$.

The square of the angular momentum operator $\hat{L}^2$ has the eigenvalues $\hbar^2 l(l+1)$ and normalized eigenfunctions given by the spherical harmonics $Y_l^m(\nu,\phi)$. Since the set $\{Y_l^m\}$ represents a complete orthonormal basis over the spherical domain, the wave function ξ can be expanded in such a basis. But, as we are looking for the unique lowest-energy state, which is represented by a ϕ-independent real function $\xi(\nu)$, its expansion becomes

$$\xi(\nu) = \frac{\sqrt{N}}{A}\sum_i c_i Y_i^0(\nu), \tag{60}$$

so that the normalization reduces to $\sum_i |c_i|^2 = 1$. In the following we use an important property of the spherical harmonics Y_l^m, which reads $\cos(\nu) Y_l^m = \alpha_l^m Y_{l-1}^m + \alpha_{l+1}^m Y_{l+1}^m$ with the abbreviation $\alpha_l^m = \sqrt{\frac{(l-m)(l+m)}{(2l-1)(2l+1)}}$. With this we get

$$\cos^2(\nu) Y_l^m = \alpha_l^m \alpha_{l-1}^m Y_{l-2}^m + \left[(\alpha_l^m)^2 + \left(\alpha_{l+1}^m\right)^2 \right] Y_l^m + \alpha_{l+2}^m \alpha_{l+1}^m Y_{l+2}^m. \tag{61}$$

Taking these properties in (59) into account leads to

$$\varepsilon_i c_i + \lambda \sum_j M_{ij} c_j + 4\pi g_{\text{eff}} \sum_{jkl} \Gamma_{ijkl} c_j c_k c_l = \mu c_i, \tag{62}$$

where we define the effective interaction strength $g_{\text{eff}} = \bar{g}_{2D} N / 4\pi A^2$. Furthermore, we introduce the abbreviations

$$\varepsilon_l = \frac{\hbar^2 l(l+1)}{2mA^2}, \tag{63}$$

$$M_{ij} = 2\pi \int_0^\pi d\nu \, \sin(\nu) Y_i^0(\nu) Y_j^0(\nu) \cos^2(\nu), \tag{64}$$

$$\Gamma_{ijkl} = 2\pi \int_0^\pi d\nu \, \sin(\nu) Y_i^0(\nu) Y_j^0(\nu) Y_k^0(\nu) Y_l^0(\nu), \tag{65}$$

which have the specific values

$$\Gamma_{ij00} = \frac{1}{4\pi} \delta_{ij}, \quad M_{i0} = \frac{1}{3} \delta_{i0} + \frac{2}{3\sqrt{5}} \delta_{i,2}, \tag{66}$$

where δ_{ij} denotes the Kroenecker delta.

Now we apply a generalization of Rayleigh–Schrödinger perturbation theory [57–60] in order to solve the nonlinear equation (62) perturbatively. To this end we employ the Taylor expansions of both the expansion coefficients c_i and the chemical potential μ with respect to the dimensionless smallness parameter λ:

$$c_i = c_i^{(0)} + \lambda c_i^{(1)} + \lambda^2 c_i^{(2)} + \cdots, \qquad \mu = \mu^{(0)} + \lambda \mu^{(1)} + \lambda^2 \mu^{(2)} + \cdots. \tag{67}$$

Considering the zeroth-order solution, we find $c_i^{(0)} = \delta_{i,0}$ and $\mu^{(0)} = g_{\text{eff}}$.

In order to use the same normalization as in Rayleigh–Schrödinger perturbation theory, we follow reference [57] and define the renormalization constant $Z(\lambda)$ according to

$$a_i = Z c_i, \tag{68}$$

so we get

$$|Z|^2 = \sum_i |a_i|^2. \tag{69}$$

The new coefficients a_i are then normalized by $\sum_i a_i c_i^{(0)} = a_0 = 1$. Furthermore, with this Equation (62) becomes

$$\varepsilon_i a_i + \lambda \sum_j M_{ij} a_j + \frac{4\pi g_{\text{eff}}}{|Z|^2} \sum_{jkl} \Gamma_{ijkl} a_j a_k a_l = \mu a_i, \tag{70}$$

with the corresponding expansion

$$a_i = a_i^{(0)} + \lambda a_i^{(1)} + \lambda^2 a_i^{(2)} + \cdots. \tag{71}$$

Note that here the coefficients $a_i^{(l)}$ depend on $|Z|^2$. Therefore, we treat $|Z|^2$ as another constant and expand the results according to (68) and (69) at the end. In addition, since $a_0 = 1$, we have

$$a_0^{(n)} = 0, \qquad n > 0, \tag{72}$$

which implies that $|Z|^2 = 1 + O(\lambda^2)$. Thus, if one is interested only in first-order perturbation theory, one could consider $|Z|^2$ equal to 1.

Substituting (71) into (70) and applying (66), we get

$$\varepsilon_i a_i^{(n)} + \sum_j M_{ij} a_j^{(n-1)} + 3\frac{g_{\text{eff}}}{|Z|^2} a_i^{(n)} + \frac{4\pi g_{\text{eff}}}{|Z|^2} \sum_{\substack{j,k,l \\ r,s,t<n}} \Gamma_{ijkl} a_j^{(r)} a_k^{(s)} a_l^{(t)} \delta_{r+s+t,n}$$
$$= \mu^{(0)} a_i^{(n)} + \sum_{m=1}^{n} \mu^{(m)} a_i^{(n-m)}. \tag{73}$$

Considering $i = 0$ in (73), we obtain a recursion relation for the respective perturbative orders of the chemical potential $\mu^{(n)}$

$$\mu^{(n)} = \sum_j M_{0j} a_j^{(n-1)} + \frac{4\pi g_{\text{eff}}}{|Z|^2} \sum_{\substack{j,k,l \\ r,s,t<n}} \Gamma_{0jkl} a_j^{(r)} a_k^{(s)} a_l^{(t)} \delta_{r+s+t,n}, \tag{74}$$

while for $i > 0$ in (73), we get a recursion relation for the perturbative coefficients $a_i^{(n)}$

$$a_i^{(n)} = \frac{1}{\varepsilon_i - \mu_0 + \frac{3g_{\text{eff}}}{|Z|^2}} \Bigg[-\sum_j M_{ij} a_j^{(n-1)} - \frac{g_{\text{eff}}}{|Z|^2} \sum_{\substack{j,k,l \\ r,s,t<n}} \Gamma_{ijkl} a_j^{(r)} a_k^{(s)} a_l^{(t)} \delta_{r+s+t,n} + \sum_{m=1}^{n} \mu^{(m)} a_i^{(n-m)} \Bigg]. \tag{75}$$

Note that in the linear case, where we have $g_{\text{eff}} = 0$, equations (74) and (75) reduce to the usual Rayleigh–Schrödinger recursion formulae, where the normalization constant Z does not appear. Furthermore, we read off from (74) and (75) the first-order perturbative result for $i > 0$

$$\mu^{(1)} = M_{00} = \frac{1}{3}, \tag{76}$$
$$a_i^{(1)} = -\frac{1}{\varepsilon_i - \mu_0 + \frac{3g_{\text{eff}}}{|Z|^2}} M_{i0} = -\frac{1}{\varepsilon_2 + \frac{(3-|Z|^2)g_{\text{eff}}}{|Z|^2}} \frac{2}{3\sqrt{5}} \delta_{i2}. \tag{77}$$

Since we have $|Z|^2 = 1 + O(\lambda^2)$, we conclude from (68)

$$c_i = \delta_{i0} - \lambda \tfrac{1}{\varepsilon_2 + 2g_{\text{eff}}} \tfrac{2}{3\sqrt{5}} \delta_{i2} + O\left(\lambda^2\right), \tag{78}$$

which gives for the ground state wave function according to (60)

$$\xi_0(\nu) = \sqrt{\frac{N}{4\pi A^2}} \left[1 - \lambda \frac{1}{\varepsilon_2 + 2g_{\text{eff}}} \left(\cos^2 \nu - \frac{1}{3} \right) \right] + O\left(\lambda^2\right). \tag{79}$$

In addition we obtain from (74) the second-order correction for the chemical potential:

$$\mu^{(2)} = -\left(\frac{2}{3\sqrt{5}} \right)^2 \frac{1}{\varepsilon_2 + 2g_{\text{eff}}} + 3g_{\text{eff}} \left(\frac{2}{3\sqrt{5}} \right)^2 \frac{1}{(\varepsilon_2 + 2g_{\text{eff}})^2}. \tag{80}$$

In order to determine the range of validity for these perturbative results, we performed a comparative analysis, as depicted in figure 2. To this end we examined the chemical potential and the wave-function coefficients, as defined in equation (60), and contrasted them with the results obtained from a numerical solution of equation (62) using the relaxation method. Thus, we read off that first-order perturbative results are indistinguishable from the numerical ones for surface eccentricities $\bar{\epsilon} < 2\hbar/m\Omega_0 A^2$.

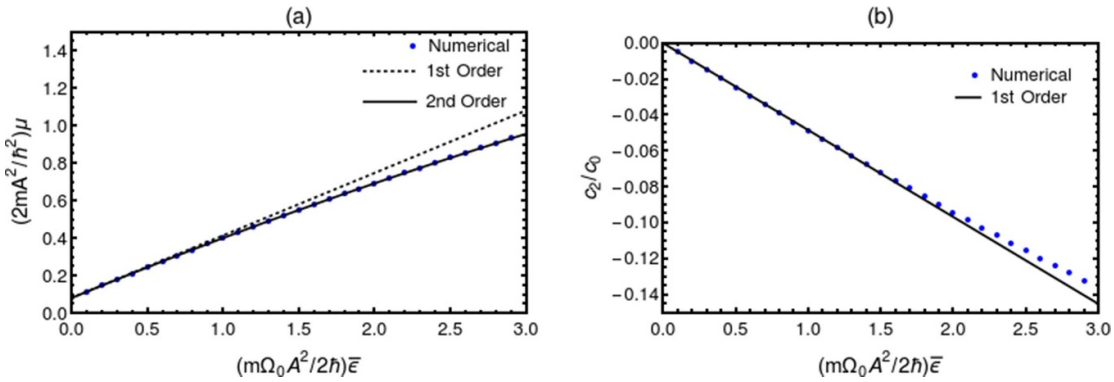

Figure 2. (a) Chemical Potential μ as a function of the surface eccentricity $\bar{\epsilon}$ for $2mN\bar{g}_{2D}/\hbar^2 = 1$. Black dashed and solid line represent analytical results corresponding to first- and second-order perturbation theory according to equations (76) and (80), respectively. Blue dots are obtained by numerically by solving equation (62). (b) Ratio between the coefficients c_2 and c_0 as a function of the surface eccentricity $\bar{\epsilon}$ according to equation (60) for $2mN\bar{g}_{2D}/\hbar^2 = 1$. The black solid line corresponds to the first-order perturbative result in equation (78), while blue dots are obtained from a numerical solution of equation (62).

6.2. Perturbative excitation spectrum

We consider now the dynamics of small excitations over the ground state $\xi^{(0)}$, which are described by the time-dependent GP equation

$$\frac{1}{2mA^2}\hat{L}^2\xi + \lambda\cos^2(\nu)\,\xi + \bar{g}_{2D}\left|\xi\right|^2\xi = i\hbar\frac{\partial\xi}{\partial t} \tag{81}$$

and the ansatz $\xi(t) = e^{-i\mu t/\hbar}[\xi_0 + \delta\xi(t)]$. Here $\delta\xi(t) = ue^{-i\omega t} - \bar{u}^* e^{i\omega t}$ represent small elongations out of the ground state, yielding the Bogoliubov equations [61]

$$TU = \hbar\omega\,\sigma U, \tag{82}$$

where we have introduced the abbreviations

$$T = \begin{pmatrix} \frac{1}{2mA^2}\hat{L}^2 + \lambda\cos^2(\nu) + 2\bar{g}_{2D}\left|\xi_0\right|^2 - \mu & -\bar{g}_{2D}\left|\xi_0\right|^2 \\ -\bar{g}_{2D}\left|\xi_0\right|^2 & \frac{1}{2mA^2}\hat{L}^2 + \lambda\cos^2(\nu) + 2\bar{g}_{2D}\left|\xi_0\right|^2 - \mu \end{pmatrix}, \tag{83}$$

$$\sigma = \begin{pmatrix} 1 & 0 \\ 0 & -1 \end{pmatrix}, \tag{84}$$

$$U = \begin{pmatrix} u \\ \bar{u} \end{pmatrix}. \tag{85}$$

According to [62, 63], we can apply a generalized version of Rayleigh–Schrödinger perturbation theory to the generalized eigenvalue problem (82).

To this end, we must expand (83) in a power series of λ

$$T = T_0 + \lambda T_1 + O\left(\lambda^2\right). \tag{86}$$

From (76) and (79), we have

$$T_0 = \begin{pmatrix} \frac{1}{2mA^2}\hat{L}^2 + \frac{\bar{g}_{2D}N}{4\pi A^2} & -\frac{\bar{g}_{2D}N}{4\pi A^2} \\ -\frac{\bar{g}_{2D}N}{4\pi A^2} & \frac{1}{2mA^2}\hat{L}^2 + \frac{\bar{g}_{2D}N}{4\pi A^2} \end{pmatrix}, \tag{87}$$

$$T_1 = \left(1 - 4\frac{\bar{g}_{2D}N}{4\pi A^2}\frac{1}{\frac{3\hbar^2}{mA^2} + \frac{\bar{g}_{2D}N}{2\pi A^2}}\right)\left(\cos^2\nu - \frac{1}{3}\right)\begin{pmatrix} 1 & 0 \\ 0 & 1 \end{pmatrix} + 2\frac{\bar{g}_{2D}N}{4\pi A^2}\frac{1}{\frac{3\hbar^2}{mA^2} + \frac{\bar{g}_{2D}N}{2\pi A^2}}\left(\cos^2\nu - \frac{1}{3}\right)\begin{pmatrix} 0 & 1 \\ 1 & 0 \end{pmatrix}. \tag{88}$$

Let us now express the problem in the basis of the spherical harmonics $\{Y_l^m\}$, i.e.

$$U(\nu,\phi) = \sum_{lm} c_{(l,m)}\,Y_l^m(\nu,\phi), \tag{89}$$

where the expansion coefficients are given by

$$c_{(l,m)} = \int_0^{\pi} d\nu \sin\nu \int_0^{2\pi} d\phi\, Y_l^m(\nu,\phi)^*\, U(\nu,\phi)\,. \tag{90}$$

Thus, the operator T is represented in the basis of the spherical harmonics via the matrix elements

$$T^{(l,m),(l',m')} = \int_0^{\pi} d\nu \sin\nu \int_0^{2\pi} d\phi\, Y_l^m(\nu,\phi)^*\, T Y_{l'}^{m'}(\nu,\phi)\,. \tag{91}$$

From (87) we then deduce at zeroth order

$$T_0^{(l,m),(l',m')} = \begin{pmatrix} \varepsilon_l + g_{\text{eff}} & -g_{\text{eff}} \\ -g_{\text{eff}} & \varepsilon_l + g_{\text{eff}} \end{pmatrix} \delta_{l,l'}\delta_{m,m'}, \tag{92}$$

while (61) and (88) yield the corresponding first-order contribution for T:

$$\begin{aligned} T_1^{(l,m),(l',m')} = &\left(1 - 4g_{\text{eff}}\frac{1}{\varepsilon_2 + 2g_{\text{eff}}}\right) \times \begin{pmatrix} 1 & 0 \\ 0 & 1 \end{pmatrix} \\ &\times \left(\alpha_l^m \alpha_{l-1}^m \delta_{l,l'-2} + \left[(\alpha_l^m)^2 + (\alpha_{l+1}^m)^2\right]\delta_{l,l'} + \alpha_{l+2}^m \alpha_{l+1}^m \delta_{l,l'+2} - \frac{1}{3}\delta_{l,l'}\right)\delta_{m,m'} \\ &+ 2g_{\text{eff}}\frac{1}{\varepsilon_2 + 2g_{\text{eff}}} \times \begin{pmatrix} 0 & 1 \\ 1 & 0 \end{pmatrix} \\ &\times \left(\alpha_l^m \alpha_{l-1}^m \delta_{l,l'-2} + \left[(\alpha_l^m)^2 + (\alpha_{l+1}^m)^2\right]\delta_{l,l'} + \alpha_{l+2}^m \alpha_{l+1}^m \delta_{l,l'+2} - \frac{1}{3}\delta_{l,l'}\right)\delta_{m,m'}. \end{aligned} \tag{93}$$

A direct diagonalization of (92) yields for the eigenvalues for each $(l,\ m)$

$$\hbar\left(\omega_{\pm}^{(l,m)}\right)_0 = \pm\sqrt{\varepsilon_l(\varepsilon_l + 2g_{\text{eff}})}, \tag{94}$$

with the corresponding eigenvectors

$$\left(c_{(l',m')}^{(l,m)}\right)_0 = \begin{pmatrix} \frac{g_{\text{eff}} + \varepsilon_l \pm \sqrt{\varepsilon_l(\varepsilon_l + 2g_{\text{eff}})}}{g} \\ 1 \end{pmatrix} \delta_{l,l'}\delta_{m,m'}. \tag{95}$$

The first-order correction to the eigenvalues $\hbar\omega_{\pm}^{(l,m)}$ is then be determined from the generalized Rayleigh–Schröedinger theory, i.e.

$$\hbar\left(\omega_{\pm}^{(l,m)}\right)_1 = \frac{\langle U_{\pm}^{(0)} | T_1 | U_{\pm}^{(0)}\rangle}{\langle U_{\pm}^{(0)} | \sigma | U_{\pm}^{(0)}\rangle}, \tag{96}$$

which becomes in the basis of the spherical harmonics $\{Y_l^m\}$

$$\hbar\left(\omega_{\pm}^{(l,m)}\right)_1 = \frac{\sum_{(l',m'),(l'',m'')} \left(c_{(l'',m'')}^{(l,m)}\right)_0^{\dagger} T_1^{(l'',m''),(l',m')} \left(c_{(l',m')}^{(l,m)}\right)_0}{\sum_{(l',m')} \left(c_{(l',m')}^{(l,m)}\right)_0^{\dagger} \sigma \left(c_{(l',m')}^{(l,m)}\right)_0}. \tag{97}$$

Using (93), we have concretely

$$\hbar\left(\omega_{\pm}^{(l',m')}\right)_1 = \pm\frac{\left[(\alpha_l^m)^2 + (\alpha_{l+1}^m)^2 - \frac{1}{3}\right]\left[g_{\text{eff}}\ (\varepsilon_2 - 2\varepsilon_l) + \varepsilon_l\varepsilon_2\right]}{(2g_{\text{eff}} + \varepsilon_2)\sqrt{\varepsilon_l(\varepsilon_l + 2g_{\text{eff}})}}. \tag{98}$$

With this, we obtain the final expression for the excitation frequencies:

$$\omega_{\pm}^{(l,m)} = \pm\sqrt{\varepsilon_l(\varepsilon_l + 2g_{\text{eff}})} \pm \lambda\frac{\left[(\alpha_l^m)^2 + (\alpha_{l+1}^m)^2 - \frac{1}{3}\right]\left[g_{\text{eff}}\ (\varepsilon_2 - 2\varepsilon_l) + \varepsilon_l\varepsilon_2\right]}{(2g_{\text{eff}} + \varepsilon_2)\sqrt{\varepsilon_l(\varepsilon_l + 2g_{\text{eff}})}} + O\left(\lambda^2\right). \tag{99}$$

In order to assess the validity range of the first-order perturbative result in equation (99), we compare some eigenvalues as shown in figure 3 with the corresponding results obtained through direct numerical

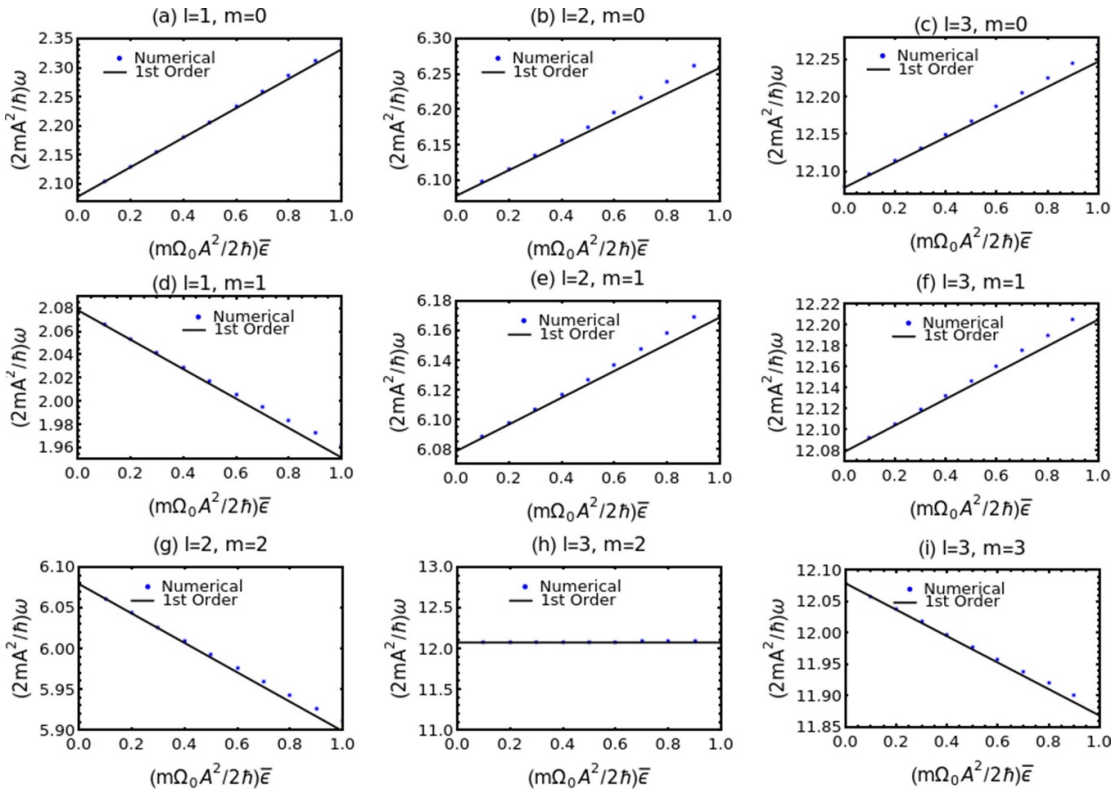

Figure 3. Comparison of excitation frequencies between the first-order perturbative results in equation (99) and the eigenvalues obtained through direct numerical diagonalization of equation (82) for varying values of l and m for $2mN\bar{g}_{2D}/\hbar^2 = 1$. The figure demonstrates the validity range of the perturbative approximation and highlights an intriguing case for $l = 3$ and $m = 2$ (shown as figure (h)), where the first-order correction vanishes and the eccentricity of the trap has no effect on the corresponding eigenfrequency.

diagonalization of equation (82). An intriguing behavior arises when considering the case of $l = 3$ and $m = 2$, which corresponds to figure 3(h). For these specific values of l and m, the first-order correction in equation (99) vanishes, i.e. changes in the eccentricity of the trap have no effect on the eigenfrequency. Thus, only higher-order corrections could potentially change the eigenfrequency. To date, we have no explanation for this occurrence, which is limited to such specific l and m values, nor have we determined if this result holds true for all eccentricity values. Further investigation is needed to comprehend this phenomenon. In addition, such results are consistent with references [31, 33] for $\bar{\epsilon} = 0$, when their thin-shell limit is considered.

7. Summary and conclusions

In this paper, we have shown how the parameters of a bubble trap have to be carefully chosen in order to allow the existence of a thin-shell limit. Under the adequate assumptions, we were able to perform a dimensional compactification which leads to an effective 2D Hamiltonian for interacting BECs. From the experimental point of view, we demonstrated that, in order to avoid the collapse of the condensate, the thin-shell limit must be taken in such way that the spatial distortion caused by the eccentricity of the surface must be kept in the same order of magnitude as the width of the Gaussian distribution perpendicular to the surface. Details on how the experimentally obtained bubble-trap potentials fit into our general theory were also provided. In addition, applications of this theory to stationary systems as well as the excitation frequencies were calculated.

Data availability statement

All data that support the findings of this study are included within the article (and any supplementary files).

Acknowledgments

This work was supported by CNPq (Conselho Nacional de Desenvolvimento Científico e Tecnológico), and DAAD-CAPES PROBRAL, Brazil Grant Number 88887.627948/2021-00. N S M acknowledges Štefan Schwarz Support Fund, Projects OPTIQUTE APVV-18-0518, QUASIMODO VEGA 2/0156/22, and Grant No. 61466 from the John Templeton Foundation, as part of 'The Quantum Information Structure of Spacetime (QISS)' Project (qiss.fr). The opinions expressed in this publication are those of the author(s) and do not necessarily reflect the views of the John Templeton Foundation. N S M thanks Nana Siddharth and Seyed Arash Ghoreishi for pointing out useful bibliography. Furthermore, A P acknowledges financial support by the Deutsche Forschungsgemeinschaft (DFG) via the Collaborative Research Center SFB/TR185 (Project No. 277625399).

Appendix. Derivation of constants in H_0

It is necessary to specify some constants appearing for the Hamiltonian H_0. In order to do that, let us use the formula for the derivatives of the determinant of a quantity B

$$\begin{cases} \frac{d|B|}{d\lambda} = |B|\mathrm{Tr}\left(B^{-1}\frac{dB}{d\lambda}\right), \\ \frac{d^2|B|}{d\lambda^2} = |B|\mathrm{Tr}\left(B^{-1}\frac{dB}{d\lambda}\right)^2 + |B|\mathrm{Tr}\left(B^{-1}\frac{d^2B}{d\lambda^2}\right) - |B|\mathrm{Tr}\left(B^{-1}\frac{dB}{d\lambda}B^{-1}\frac{dB}{d\lambda}\right). \end{cases} \tag{A.1}$$

With this the metric g has the following Taylor series up to second order

$$g(s,\epsilon) = g_0 + g_1\Lambda^{-1/2}y + g_\epsilon\Lambda^{-1}\bar{\epsilon} + \frac{1}{2}g_2\Lambda^{-1}y^2 + O\left(\Lambda^{-3/2}\right), \tag{A.2}$$

where we have $g(0,0) = g_0$, $\frac{\partial g(0,0)}{\partial s} = g_1$, $\frac{\partial g(0,0)}{\partial \epsilon} = g_\epsilon$, and $\frac{\partial^2 g(0,0)}{\partial s^2} = g_2$. Thus, the derivatives of γ can be expressed as $\gamma_1 = \mathrm{Tr}(g_0^{-1}g_1)$ and $\gamma_2 = \mathrm{Tr}(g_0^{-1}g_1)^2 + \mathrm{Tr}(g_0^{-1}g_2) - \mathrm{Tr}(g_0^{-1}g_1g_0^{-1}g_1)$. In the thin-shell limit the metric becomes the spherical one, yielding

$$g_0 = \begin{pmatrix} 1 & 0 & 0 \\ 0 & A^2 & 0 \\ 0 & 0 & A^2\sin^2\nu \end{pmatrix}, \; g_1 = \begin{pmatrix} 0 & 0 & 0 \\ 0 & 2A & 0 \\ 0 & 0 & 2A\sin^2\nu \end{pmatrix}, \; g_2 = \begin{pmatrix} 0 & 0 & 0 \\ 0 & 2 & 0 \\ 0 & 0 & 2\sin^2\nu \end{pmatrix}. \tag{A.3}$$

This can be used to calculate the traces, granting $\gamma_1 = 4/A$ and $\gamma_2 = 12/A^2$.

ORCID iD

Natália S Móller https://orcid.org/0000-0003-0949-9023

References

[1] Anderson M H, Ensher J R, Matthews M R, Wieman C E and Cornell E A 1995 Observation of Bose-Einstein condensation in a dilute atomic vapor *Science* **269** 5221
[2] Davis K B, Mewes M O, Andrews M R, van Druten N J, Durfee D S, Kurn D M and Ketterle W 1995 Bose-Einstein condensation in a gas of sodium atoms *Phys. Rev. Lett.* **75** 22
[3] Zobay O and Garraway B M 2000 Properties of coherent matter-wave bubbles *Acta Phys. Slovaca* **50** 359–67
[4] Zobay O and Garraway B M 2001 Two-dimensional atom trapping in field-induced adiabatic potentials *Phys. Rev. Lett.* **86** 1195
[5] Zobay O and Garraway B M 2004 Atom trapping and two-dimensional Bose-Einstein condensates in field-induced adiabatic potentials *Phys. Rev.* A **69** 023605
[6] Lundblad N *et al* 2023 Perspective on quantum bubbles in microgravity *Quantum Sci. Technol.* **8** 024003
[7] Tononi A and Salasnich L 2023 Low-dimensional quantum gases in curved geometries *Nat. Rev. Phys.* **5** 398
[8] Colombe Y, Knyazchyan E, Morizot O, Mercier B, Lorent V and Perrin H 2004 Ultracold atoms confined in rf-induced two-dimensional trapping potentials *Europhys. Lett.* **67** 593
[9] Garraway B M and Perrin H 2016 Recent developments in trapping and manipulation of atoms with adiabatic potentials *J. Phys. B: At. Mol. Opt. Phys.* **49** 172001
[10] Perrin H and Garraway B M 2017 Trapping atoms with radio frequency adiabatic potentials *Adv. At. Mol. Opt. Phys.* **66** 181
[11] White M, Gao H, Pasienski M and DeMarco B 2006 Bose-Einstein condensates in rf-dressed adiabatic potentials *Phys. Rev.* A **74** 023616
[12] Merloti K, Dubessy R, Longchambon L, Perrin A, Pottie P E, Lorent V and Perrin H 2013 A two-dimensional quantum gas in a magnetic trap *New J. Phys.* **15** 033007
[13] van Zoest T *et al* 2010 Bose-Einstein condensation in microgravity *Science* **328** 5985
[14] Condon G *et al* 2019 All-optical Bose-Einstein condensates in microgravity *Phys. Rev. Lett.* **123** 240402
[15] Elliott E R, Krutzik M C, Williams J R, Thompson J R and Aveline D C 2018 NASA's Cold Atom Lab (CAL): system development and ground test status *npj Microgravity* **4** 16

[16] Aveline D C et al 2020 Observation of Bose-Einstein condensates in an Earth-orbiting research lab Nature 582 7811
[17] Becker D et al 2018 Space-borne Bose-Einstein condensation for precision interferometry Nature 562 7727
[18] Lundblad N 2017 Microgravity dynamics of bubble-geometry Bose-Einstein condensates (available at: https://taskbook.nasaprs.com/Publication/index.cfm?action=public_query_taskbook_content&TASKID=11095)
[19] Lundblad N, Carollo R A, Lannert C, Gold M J, Jiang X, Paseltiner D, Sergay N and Aveline D C 2019 Shell potentials for microgravity Bose-Einstein condensates Microgravity 5 1
[20] Frye K et al 2021 The Bose-Einstein condensate and cold atom laboratory EPJ Quantum Technol. 8 1
[21] Carollo R A, Aveline D C, Rhyno B, Vishveshwara S, Lannert C, Murphree J D, Elliott E R, Williams J R, Thompson R J and Lundblad N 2022 Observation of ultracold atomic bubbles in orbital microgravity Nature 606 7913
[22] Cho A 2017 Trapped in orbit Science 357 986–89
[23] Guo Y, Gutierrez E M, Rey D, Badr T, Perrin A, Longchambon L, Bagnato V S, Perrin H and Dubessy R 2022 Expansion of a quantum gas in a shell trap New J. Phys. 24 093040
[24] Shibata K, Ikeda H, Suzuki R and Hirano T 2020 Compensation of gravity on cold atoms by a linear optical potential Phys. Rev. Res. 2 013068
[25] Wolf A, Boegel P, Meister M, Balaž A, Gaaloul N and Efremov M A 2022 Shell-shaped Bose-Einstein condensates based on dual-species mixtures Phys. Rev. A 106 013309
[26] Jia F, Huang Z, Qiu L, Zhou R, Yan Y and Wang D 2022 Expansion dynamics of a shell-shaped Bose-Einstein condensate Phys. Rev. Lett. 129 243402
[27] Moller N S, dos Santos F E A, Bagnato V S and Pelster A 2020 Bose-Einstein condensation on curved manifolds New J. Phys. 22 063059
[28] Lannert C, Wei T C and Vishvehswara S 2007 Dynamics of condensate shells: collective modes and expansion Phys. Rev. A 75 013611
[29] Prestipino S and Giaquinta P V 2019 Ground state of weakly repulsive soft-core bosons on a sphere Phys. Rev. A 99 063619
[30] Bereta S J, Madeira L, Caracanhas M A and Bagnato V S 2019 Bose-Einstein condensation in spherically symmetric traps Am. J. Phys. 87 924–34
[31] Tononi A and Salasnich L 2019 Bose-Einstein condensation on the surface of a sphere Phys. Rev. Lett. 123 160403
[32] Tononi A, Cinti F and Salasnich L 2020 Quantum bubbles in microgravity Phys. Rev. Lett. 125 010402
[33] Sun K, Padavic K, Yang F, Vishveshwara S and Lannert C 2018 Static and dynamic properties of shell-shaped condensates Phys. Rev. A 98 013609
[34] Padavić K, Sun K, Lannert C and Vishveshwara S 2018 Physics of hollow Bose-Einstein condensates Europhys. Lett. 120 20004
[35] de Castro Diniz P, Oliveira E A B, Lima A R P and de Lima Henn E A 2020 Ground state and collective excitations of a dipolar Bose-Einstein condensate in a bubble trap Sci. Rep. 10 1
[36] Zhang J and Ho T L 2018 Potential scattering on a spherical surface J. Phys. B 51 115301
[37] Mitra K, Williams C J and Sa de Melo C A R 2008 Superfluid and Mott-insulating shells of bosons in harmonically conned optical lattices Phys. Rev. A 77 033607
[38] Tononi A, Pelster A and Salasnich L 2022 Topological superfluid transition in bubble-trapped condensates Phys. Rev. Res. 4 013122
[39] Pará Y, Palumbo G and Macri T 2021 Probing non-Hermitian phase transitions in curved space via quench dynamics Phys. Rev. B 103 155417
[40] Caracanhas M A, Massignan P and Fetter A L 2022 Superfluid vortex dynamics on an ellipsoid and other surfaces of revolution Phys. Rev. A 105 023307
[41] Bereta S J, Caracanhas M A and Fetter A L 2021 Superfluid vortex dynamics on a spherical film Phys. Rev. A 103 053306
[42] Dritschel D G and Boatto S 2015 The motion of point vortices on closed surfaces Proc. R. Soc. A 471 20140890
[43] Hally D 1980 Stability of streets of vortices on surfaces of revolution with a reflection symmetry J. Math. Phys. 21 211–17
[44] Castilho C and Machado H 2008 The N-vortex problem on asymmetric ellipsoid: a perturbation approach J. Math. Phys. 49 022703
[45] Rodrigues A R, Castilho C and Koiller J 2018 Vortex pairs on a triaxial ellipsoid and Kimura's conjecture J. Geom. Mech. 10 189–202
[46] Turner A M, Vitelli V and Nelson D R 2010 Vortices on curved surfaces Rev. Mod. Phys. 82 1301
[47] Padavić K, Sun K, Lannert C and Vishveshwara S 2020 Vortex-antivortex physics in shell shaped Bose-Einstein condensates Phys. Rev. A 102 043305
[48] Kühnel W 2002 Differential Geometry: Curves-Surfaces-Manifolds 2nd edn (American Mathematical Society)
[49] Lee J M 2000 Introduction to Topological Manifolds (Springer)
[50] Lee J M 2009 Manifolds and Differential Geometry, Graduate Studies in Mathematics (American Mathematical Society)
[51] Weisstein E W Smooth manifold (available at: https://mathworld.wolfram.com/SmoothManifold.html)
[52] Whitney H 1936 Differentiable manifolds Ann. Math. 37 645–80
[53] Smoller J and Temple B 1994 Shock-wave solutions of the Einstein equations: the Oppenheimer-Snyder model of gravitational collapse extended to the case of non-zero pressure arch Ration. Mech. Anal. 128 249–97
[54] Iofa M Z 2016 Kodama-Schwarzschild versus Gaussian normal coordinates picture of thin-shells Adv. High Energy Phys. 2016 5632734
[55] Moon P H and Spencer D E 1988 Field Theory Handbook: Including Coordinate Systems, Differential Equations and Their Solutions 2nd edn (Springer)
[56] Morse P M and Feshbach H 1953 Methods of Theoretical Physics, Part I (McGraw-Hill)
[57] Surján P R and Ángyán J 1983 Perturbation theory for nonlinear time-independent Schrödinger Phys. Rev. A 28 45
[58] Vrscay E R 1988 Nonlinear 'self-interaction' Hamiltonians of the form $H^{(}0) + \lambda\langle r^p\rangle r^q$ and their Rayleigh-Schrödinger perturbation expansions J. Math. Phys. 29 901
[59] Ángyán J G 1993 Rayleigh-Schrödinger perturbation theory for nonlinear Schrödinger equations with linear perturbation Int. J. Quantum Chem. 47 469
[60] Griffiths D 2004 Introduction to Quantum Mechanics 2nd edn (Prentice Hall)
[61] Pethick C J and Smith H 2008 Bose-Einstein Condensation in Dilute Gases (Cambridge University Press)
[62] Peters G and Wilkinson J H 1970 A x = λ B x and the generalized eigenproblem SIAM J. Numer. Anal. 7 4
[63] Bender C M 2007 Making sense of non-Hermitian Hamiltonians Rep. Prog. Phys. 70 947